

Nonreciprocal Magnon by Symmetric Anisotropic Exchange Interaction in Honeycomb Antiferromagnet

Takuya Matsumoto

Department of Physics, Hokkaido University, Sapporo 060-0810, Japan

Satoru Hayami

Department of Applied Physics, The University of Tokyo, Tokyo 113-8656, Japan

(Dated: May 29, 2020)

We investigate a microscopic origin of nonreciprocal magnon that is distinct from the Dzyaloshinskii-Moriya interaction in a honeycomb antiferromagnet. The key ingredient is a symmetric anisotropic exchange interaction depending on the bond direction, which results in a valley-type nonreciprocal magnon excitations under the staggered antiferromagnetic ordering. Furthermore, we find this type of nonreciprocal magnon exhibits a peculiar magnetic-field response; the nonreciprocal direction can be manipulated by the in-plane rotating magnetic field. The obtained results can be accounted for the emergence of the magnetic toroidal multipoles.

I. INTRODUCTION

Magnetism in the absence of the spatial inversion symmetry has drawn considerable interest in condensed matter physics, since it exhibits various fascinating phenomena, such as the magneto-electric effect [1–3] and nonreciprocal transport [4]. For example, magnetic skyrmions in polar/chiral magnets show nonreciprocal directional dichroism due to the lack of the spatial inversion symmetry [5]. Recently, current-induced magnetization and magneto-piezo electricity in antiferromagnetic (AFM) metals without the inversion symmetry have been observed in experiments [6–8].

Such magnets without the spatial inversion symmetry also affect collective excitations of magnon and photon, which results in directional-dependent dynamical properties even in magnetic insulators [9–16]. Theoretically, the nonreciprocal magnons have long been studied in the magnetic systems with the Dzyaloshinsky-Moriya (DM) interaction [17, 18], which were observed in recent experiments [19–28]. Among them, asymmetric (nonreciprocal) magnon dispersions were directly detected in the noncentrosymmetric ferromagnet LiFe_5O_8 [19] and AFM $\alpha\text{-Cu}_2\text{V}_2\text{O}_7$ [24] through the spectroscopic measurements. Furthermore, such asymmetric magnons give rise to directional-dependent physical phenomena, such as nonreciprocal magneto-optical [29–35] and nonreciprocal spin Seebeck effects [36, 37]. Meanwhile, some nonreciprocal-magnon mechanisms which are different from the DM interaction have been found, e.g., the dipolar coupling between ferromagnetic layers [38–42], the vector spin chirality in the spiral spin structures [29, 30, 32, 43], the bond-dependent symmetric anisotropic exchange interaction [44], and magnetic interactions induced by curved magnetic surfaces [45], and graded magnetization [46] in ferromagnetic films. Among them, the bond-dependent symmetric anisotropic and DM interactions originate from the spin-orbit coupling in bulk systems, which are different from each other: The former mechanism does not require the inversion

symmetry breaking on the bond center, while the latter does. Thus, nonreciprocal magnons can be realized even in centrosymmetric magnets when the magnetic order breaks the inversion symmetry in the presence of the bond-dependent symmetric anisotropic exchange interaction, which will extend the scope of functional materials toward applications to AFM spintronics devices. Nevertheless, its microscopic mechanism has not been elucidated thus far.

In the present study, we investigate the behavior of nonreciprocal magnons under the anisotropic magnetic interactions on the basis of point group symmetry. We show that the threefold bond-dependent symmetric exchange interaction in the honeycomb structure leads to a valley-type nonreciprocal magnon excitations once the staggered-type collinear AFM ordering occurs. We also find that its nonreciprocal magnon excitations show an in-plane angle-dependent directional dispersions under an external magnetic field. We present that the microscopic origin of the nonreciprocal magnon excitations is attributed to the emergent magnetic toroidal multipoles hidden in the cluster magnetic structure from the symmetry point of view.

The organization of this paper is as follows. In Sec. II, we introduce the spin model and outline the linear spin wave calculations based on the Holstein-Primakoff transformations. In Sec. III, we give the nonreciprocal magnon excitations at both zero and nonzero magnetic fields. Section IV is devoted to a summary of the present paper. In Appendix A, we present the calculations of the spin configurations in the ground state. In Appendix B, we compare the magnon dispersions obtained in the present paper with those in the presence of the DM interaction.

II. MODEL AND METHOD

Let us start by considering the localized spin model in the honeycomb structure, as shown in Fig. 1(a). By taking into account the symmetry elements of the hon-

eycomb structure under the point group $6/mmm$, the spin Hamiltonian with the symmetry-allowed exchange interactions is given by

$$\mathcal{H} = \sum_{\langle ij \rangle} \left[J(S_{iA}^+ S_{jB}^- + S_{iA}^- S_{jB}^+) + J^z S_{iA}^z S_{jB}^z + J^a (\gamma_{ij} S_{iA}^+ S_{jB}^+ + \gamma_{ij}^* S_{iA}^- S_{jB}^-) \right] - \sum_{i,\eta} \mathbf{H} \cdot \mathbf{S}_{i\eta}, \quad (1)$$

where $S_{i\eta}^\zeta$ is a classical spin with a $\zeta = x, y, z$ component at unit cell i and sublattice $\eta = A, B$, and $S_{i\eta}^\pm \equiv (S_{i\eta}^x \pm iS_{i\eta}^y)/\sqrt{2}$. The sum of $\langle ij \rangle$ is taken for the nearest-neighbor spins. The first two terms in the square bracket in Eq. (1) represent the xxz -type AFM exchange interactions where we assume $J_z > J > 0$. The third term stands for a bond-dependent symmetric anisotropic exchange interaction with the coupling constant J^a and the phase factor $\gamma_{ij} \equiv e^{i\frac{2\pi n}{3}}$ where $n = 0, 1, 2$ corresponds to the three nearest-neighbor bonds in Fig. 1(a). This term originates from the relativistic spin-orbit coupling in multi-orbital systems where the competition between the crystalline electric field and the atomic spin-orbit coupling gives rise to a Kramers doublet under the large total angular momentum, although it is different from the DM interaction which appears in the absence of the inversion symmetry at the bond center. A similar bond-dependent symmetric anisotropic exchange interaction has recently been studied in the triangle AFM [47] and honeycomb ferromagnet [48, 49]. The second term is a Zeeman interaction under an external in-plane magnetic field, $\mathbf{H} = (H_x, H_y, 0) = H(\cos \phi, \sin \phi, 0)$. We set $J^z = 1$ as the energy unit and the distance between A and B sublattices to be 1.

In order to discuss the magnon excitations, we investigate the optimal spin pattern within the two-sublattice orderings in the model in Eq. (1). For $J^z > J$, the spin configurations are given by $\mathbf{S}_{iA} = S(\sin \theta \cos \phi, \sin \theta \sin \phi, \cos \theta)$ and $\mathbf{S}_{iB} = S(\sin \theta \cos \phi, \sin \theta \sin \phi, -\cos \theta)$ where $\theta = \sin^{-1}[H/3S(J + J^z)]$, as shown in Appendix A. Note that J^a does not contribute to the ground-state energy within the two-sublattice AFM ordering, although it plays an important role in asymmetric magnon excitations as discussed in Sec. III.

For the above spin configuration, we examine magnetic excitations by using the linear spin-wave theory. We adopt the standard Holstein-Primakoff transformation as $\tilde{S}_{i\eta}^+ \equiv \sqrt{S}\eta_i^+$, $\tilde{S}_{i\eta}^- \equiv \sqrt{S}\eta_i^{\dagger}$, and $\tilde{S}_{i\eta}^z \equiv S - \eta_i^{\dagger}\eta_i^+$ where $S = 1$ and $(\tilde{S}_{i\eta}^x, \tilde{S}_{i\eta}^y, \tilde{S}_{i\eta}^z)^T$ is the local rotated frame with the quantization axis along the $\tilde{S}_{i\eta}^z$ direction and $\eta_i^+ = a_i$ and b_i are the boson operator for sublattice $\eta = A$ and B , respectively. By performing the Fourier transformation, the spin-wave Hamiltonian in momentum (\mathbf{q}) space is obtained as

$$\mathcal{H} = \frac{1}{2} \sum_{\mathbf{q}} \Psi_{\mathbf{q}}^{\dagger} \begin{pmatrix} X(\mathbf{q}) & Y(\mathbf{q}) \\ Y^*(-\mathbf{q}) & X^*(-\mathbf{q}) \end{pmatrix} \Psi_{\mathbf{q}}, \quad (2)$$

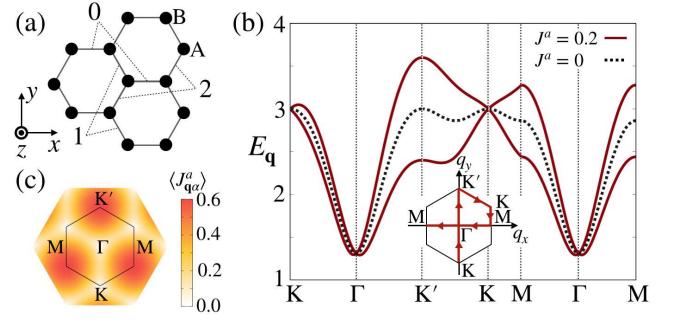


FIG. 1. (a) Schematic picture of the honeycomb structure consisting of A and B sublattices. The bond index 0-2 is also shown. (b) The magnon dispersions in the model in Eq. (2) at $J = 0.9$ and $H = 0$. The red solid (black dotted) lines represent the result at $J^a = 0.2$ ($J^a = 0$). In the inset, the first Brillouin zone is shown. (c) The color plot of $\langle J_{\mathbf{q}\alpha}^a \rangle$ in Eq. (7) in \mathbf{q} space.

where $\Psi_{\mathbf{q}}^{\dagger} = (a_{\mathbf{q}}^{\dagger}, b_{\mathbf{q}}^{\dagger}, a_{-\mathbf{q}}, b_{-\mathbf{q}})$. We omit the classical ground-state energy per unit cell $E_{\text{GS}} = -3J^z S^2 - H^2/[3(J^z + J)]$. $X(\mathbf{q})$ and $Y(\mathbf{q})$ in Eq. (2) are 2×2 matrices, which are given by

$$X(\mathbf{q}) = \begin{pmatrix} Z & \sum_n F_n e^{i\mathbf{q} \cdot \boldsymbol{\rho}_n} \\ \sum_n F_n^* e^{-i\mathbf{q} \cdot \boldsymbol{\rho}_n} & Z \end{pmatrix}, \quad (3)$$

$$Y(\mathbf{q}) = \begin{pmatrix} 0 & \sum_n G_n e^{i\mathbf{q} \cdot \boldsymbol{\rho}_n} \\ \sum_n G_n e^{-i\mathbf{q} \cdot \boldsymbol{\rho}_n} & 0 \end{pmatrix}, \quad (4)$$

where the sum of n is taken for the three nearest-neighbor bonds ($n = 0, 1, 2$) with $\boldsymbol{\rho}_0 = (1, 0)$, $\boldsymbol{\rho}_1 = (-1/2, \sqrt{3}/2)$, and $\boldsymbol{\rho}_2 = (-1/2, -\sqrt{3}/2)$. In Eqs. (3) and (4), F_n , G_n , and Z are expressed as

$$F_n = \frac{J + J^z}{2} \sin^2 \theta - J^a \left[\cos \Phi_n \frac{1 + \cos^2 \theta}{2} - i \sin \Phi_n \cos \theta \right], \quad (5)$$

$$G_n = -J + \sin^2 \theta \left[\frac{J + J^z}{2} + \frac{J^a}{2} \cos \Phi_n \right], \quad (6)$$

and $Z = H \sin \theta - 3J \sin^2 \theta + 3J^z \cos^2 \theta$ where $\Phi_n = 2\phi + \chi_n$ and $\chi_n = 0, 2\pi/3, 4\pi/3$ for $n = 0, 1, 2$. We use the numerical Bogoliubov transformation for the Hamiltonian in Eq. (2) for the magnon dispersions [50].

III. RESULT

In this section, we first show the nonreciprocal magnon excitations under a collinear AFM order in Sec. III A. Next, we discuss the nonreciprocal behavior under the external magnetic field in Sec. III B.

A. Collinear antiferromagnetic order at zero field

We show the result in the absence of the magnetic field ($H = 0$) where the staggered collinear AFM order with the moments along the z direction, i.e., $\theta = 0$, becomes the ground state. Figure 1(b) shows the magnon dispersions at $J = 0.9$, $J^a = 0.2$, and $H = 0$ (red solid lines). For comparison, we also show the magnon dispersions at $J^a = 0$ (black dotted lines). Compared to the result at $J^a = 0$, the magnon dispersions at $J^a = 0.2$ split in the entire Brillouin zone except for the Γ and K points. The splitting of magnon excitation spectrum is characterized in an asymmetric way: the magnon dispersions undergo an antisymmetric deformation with respect to \mathbf{q} for $J^a \neq 0$.

To examine the effect of J^a on the antisymmetric magnon dispersions, we calculate its contribution by evaluating the expectation value at each momentum \mathbf{q} in the the third term in the square bracket in Eq. (1), which is represented by

$$\begin{aligned} \langle J_{\mathbf{q}\zeta}^a \rangle \equiv & J^a \sum_n \langle \zeta_{\mathbf{q}} | e^{i\mathbf{q}\cdot\rho_n} (\bar{F}_n a_{\mathbf{q}}^\dagger b_{\mathbf{q}} + \bar{F}_n^* a_{-\mathbf{q}} b_{-\mathbf{q}}^\dagger) \\ & + e^{i\mathbf{q}\cdot\rho_n} \bar{G}_n (a_{\mathbf{q}}^\dagger b_{-\mathbf{q}}^\dagger + a_{-\mathbf{q}} b_{\mathbf{q}}) + \text{H.c.} | \zeta_{\mathbf{q}} \rangle, \quad (7) \end{aligned}$$

where $|\zeta_{\mathbf{q}}\rangle = \zeta_{\mathbf{q}}^\dagger |0\rangle$ stands for the eigenmode where $\zeta_{\mathbf{q}} = \alpha_{\mathbf{q}} (\beta_{\mathbf{q}})$ for the upper (lower) magnon band. \bar{F}_n and \bar{G}_n are given by $\bar{F}_n = [\cos \Phi_n (1 + \cos^2 \theta) / 2 - i \sin \Phi_n \cos \theta]$ and $\bar{G}_n = \cos \Phi_n \sin^2 \theta$. Figure 1(c) shows the color plot of $\langle J_{\mathbf{q}\alpha}^a \rangle$ in the entire \mathbf{q} space where $\langle J_{\mathbf{q}\alpha}^a \rangle \simeq -\langle J_{\mathbf{q}\beta}^a \rangle$. In Fig. 1(c), $\langle J_{\mathbf{q}\alpha}^a \rangle$ remains a threefold rotational symmetry in the form of $\sin(\sqrt{3}q_y/2)[\cos(3q_x/2) - \cos(\sqrt{3}q_y/2)]$, which is symmetric along the M- Γ line ($q_x \leftrightarrow -q_x$) and asymmetric along the K- Γ -K' line ($q_y \leftrightarrow -q_y$). Reflecting such a functional form, $\langle J_{\mathbf{q}\alpha}^a \rangle$ becomes the maximum at the K' point. The behavior of $\langle J_{\mathbf{q}\zeta}^a \rangle$ in Fig. 1(c) is consistent with the magnon-band splitting in Fig. 1(b). In fact, the magnon-band splitting $\Delta E_{\mathbf{q}}$ is related with $\langle J_{\mathbf{q}\zeta}^a \rangle$ as $\Delta E_{\mathbf{q}} = \langle J_{\mathbf{q}\alpha}^a \rangle - \langle J_{\mathbf{q}\beta}^a \rangle$.

We analytically evaluate the asymmetric magnon-band splitting $\Delta E_{\mathbf{q}}$ by using the perturbation analysis with respect to J^a . The lowest-energy correction by J^a is given by the first-order perturbation, which is obtained as

$$\Delta E_{\mathbf{q}} = |J^a| \sqrt{3 + 2 \left[\sum_{n=0,1,2} \cos \left(\mathbf{q} \cdot \boldsymbol{\rho}'_n + \frac{2\pi}{3} \right) \right]}, \quad (8)$$

where we assume $J^z \gg J$ for simplicity. In Eq. (8), $\boldsymbol{\rho}'_n$ is the next-nearest-neighbor vector as $\boldsymbol{\rho}'_0 = \boldsymbol{\rho}_0 - \boldsymbol{\rho}_1$, $\boldsymbol{\rho}'_1 = \boldsymbol{\rho}_1 - \boldsymbol{\rho}_2$, and $\boldsymbol{\rho}'_2 = \boldsymbol{\rho}_2 - \boldsymbol{\rho}_0$. Note that Eq. (8) describes $\Delta E_{\mathbf{q}} \neq \Delta E_{-\mathbf{q}}$. The expression indicates that an effective kinetic motion of magnons between the next-nearest-neighbor spins plays an important role in inducing the antisymmetric magnon-band splitting. Moreover, Eq. (8) shows that the nonreciprocal magnon dispersion

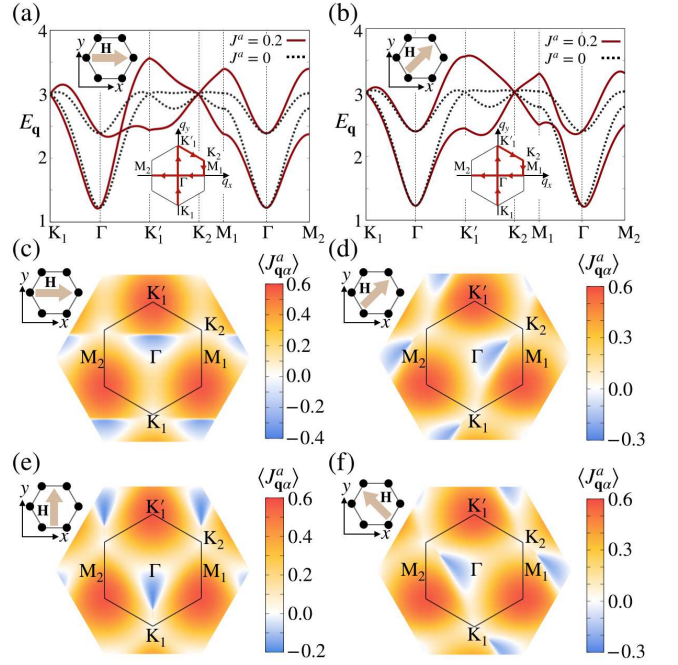


FIG. 2. (a) and (b) magnon bands at (a) $\mathbf{H} = (H, 0, 0)$ ($\phi = 0$) and (b) $\mathbf{H} = (H, H, 0)/\sqrt{2}$ ($\phi = \pi/4$) with $H = 2$. The other model parameters in Eq. (2) are the same as those in Fig. 1(b). (c)-(f) $\langle J_{\mathbf{q}\alpha}^a \rangle$ for (c) $\phi = 0$, (d) $\phi = \pi/4$, (e) $\phi = \pi/2$, and (f) $\phi = 3\pi/4$.

is proportional to the symmetric anisotropic exchange J^a and is irrespective of the sign of J^a .

Such an emergent asymmetric magnon structure in \mathbf{q} space is also caused by the DM interaction, which appears without the inversion symmetry at the bond center. However, the way of asymmetric spectra is qualitative different from each other, although both of them originate from the spin-orbit coupling microscopically. The asymmetric magnon dispersion induced by the symmetric anisotropic exchange interaction exhibits the magnon-band splitting except for the high-symmetry points, Γ and K, in Fig. 1(b), whereas that by the DM interaction does not show any splittings; the twofold degenerated bands at the K and K' points move in an opposite direction, as shown in Appendix B [13]. Thus, these two contributions are separably detected by the spectroscopic measurements [19, 24]. Moreover, another difference is found in the microscopic origin. The key issue for the present mechanism appears in the exchange interactions between the the *nearest-neighbor* bonds. On the other hand, the exchange interactions between the *next-nearest-neighbor* bonds give the contribution to nonreciprocal magnons for the mechanisms based on the DM interaction [13]. Thus, nonreciprocal magnons in the honeycomb AFM can be expected even when the next-nearest-neighbor exchange couplings including the DM interaction are negligibly small.

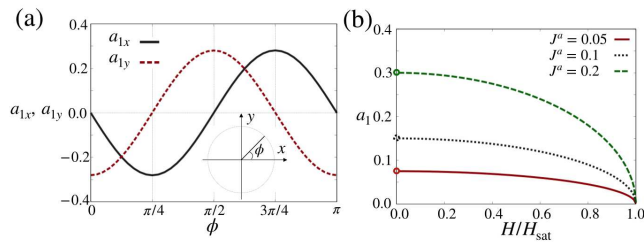


FIG. 3. (a) Magnetic-field angle dependences of the linear coefficients in the magnon band, a_{1x} and a_{1y} , at $J = 0.9$, $J^a = 0.2$, and $H = 2$. (b) H dependence of $a_1 (\equiv \sqrt{a_{1x}^2 + a_{1y}^2})$ for $J^a = 0.05, 0.1$, and 0.2 where H_{sat} represents the saturated magnetic field.

B. Canted antiferromagnetic order at nonzero field

We discuss an additional asymmetric magnon deformation under the magnetic field ($H \neq 0$). Figures 2(a) and 2(b) represent the results in the presence of the in-plane magnetic field $\mathbf{H} = H(\cos \phi, \sin \phi, 0)$ for $\phi = 0$ and $\phi = \pi/4$, respectively. The magnon dispersions in Figs. 2(a) and 2(b) are different from each other for $J^a \neq 0$, while they are the same for $J^a = 0$. For instance, the magnon bands are symmetric (asymmetric) along the M_1 - Γ - M_2 line in Fig. 2(a) [Fig. 2(b)], which means that the antisymmetric functional form depends on the magnetic-field direction.

In order to display the antisymmetric modulations under the in-plane magnetic field, we show $\langle J_{\mathbf{q}\alpha}^a \rangle$ ($\simeq -\langle J_{\mathbf{q}\beta}^a \rangle$) in Eq. (7) for several values of ϕ : $\phi = 0$ in Fig. 2(c), $\phi = \pi/4$ in Fig. 2(d), $\phi = \pi/2$ in Fig. 2(e), and $\phi = 3\pi/4$ in Fig. 2(f). In contrast to the result at $H = 0$ in Fig. 1(b), $\langle J_{\mathbf{q}\alpha}^a \rangle$ in Figs. 2(c)-2(f) breaks the threefold rotational symmetry: there are linearly antisymmetric modulations against q_y along the $[100]$ and $[010]$ field directions ($\phi = 0$ and $\phi = \pi/2$) in Figs. 2(c) and 2(e) and against q_x along the $[110]$ and $[\bar{1}10]$ field directions ($\phi = \pi/4$ and $\phi = 3\pi/4$) in Figs. 2(d) and 2(f). In contrast to the case at zero field in Sec. III A, the magnon-band splitting $\Delta E(\mathbf{q})$ is slightly deviated from $\langle J_{\mathbf{q}\alpha}^a \rangle - \langle J_{\mathbf{q}\beta}^a \rangle$ in the presence of \mathbf{H} .

We analyze additional antisymmetric modulations in the magnon dispersions by considering the $\mathbf{q} \rightarrow 0$ limit. By setting $\mathbf{q} = (q_x, q_y) = q(\cos \phi_q, \sin \phi_q)$, the magnon dispersion for upper band $E_{\mathbf{q}\alpha}$ is expanded as $E_{\mathbf{q}\alpha} = a_0 + (a_{1x} \cos \phi_q + a_{1y} \sin \phi_q)q + \mathcal{O}(q^2)$ where a_0 , a_{1x} , and a_{1y} are the expansion coefficients. We show the field-angle dependence of the linear coefficients a_{1x} and a_{1y} obtained by performing the numerical differentiation for upper band in Fig. 3(a). As clearly shown in Fig. 3(a), there are linear antisymmetric modulations in the magnon dispersions under the in-plane magnetic field. The angle dependences of a_{1x} and a_{1y} are fitted as $-\sin(2\phi)$ and $-\cos(2\phi)$, respectively, where their norm $a_1 \equiv \sqrt{a_{1x}^2 + a_{1y}^2}$ is independent of ϕ . The linear an-

tisymmetric direction is rotated by -2ϕ when the field direction is rotated by ϕ .

The result suggests that the nonreciprocal dispersion can be controlled by the magnetic-field direction, since the nonreciprocal transport is dominantly characterized by the linear antisymmetric components [34, 35, 37]. Moreover, it is noted that such an angle dependence of nonreciprocal magnon does not occur under the DM interaction that might appear in the next-nearest-neighbor bonds in the honeycomb AFM, as shown in Appendix B. Thus, the symmetric anisotropic exchange-driven nonreciprocal magnon can be detected by measuring the conductive and response tensors in the nonreciprocal magneto-optical [29–35] and spin Seebeck effects [36, 37] besides the microscopic spectroscopic measurements.

Figure 3(b) shows the H dependence of a_1 for $J^a = 0.05, 0.1$, and 0.2 where H_{sat} represents the saturated magnetic field. The value of a_1 becomes gradually small while increasing the magnetic field, and it vanishes at H_{sat} . Note that there is a finite jump of a_1 for infinitesimally small H , whose discontinuity is presumably due to the presence of the band crossing at the Γ point, as shown in Fig. 1(b). The magnitude of the linear coefficient a_1 is proportional to J^a in Fig. 3(b).

Finally, let us discuss the peculiar angle dependence of the nonreciprocal excitations in terms of emergent magnetic toroidal multipoles [51–53]. In the case of $H = 0$ where the staggered AFM state with the moments along the z direction is stabilized, this AFM state is regarded as a ferroic alignment of the odd-parity magnetic toroidal octupole with the $y(3x^2 - y^2)$ component [13, 54], which results in the $q_y(3q_x^2 - q_y^2)$ -type magnon band deformation, as shown in Fig. 1(c) [53]. This antisymmetric functional form implies that a directional nonreciprocity is coupled with the quadrupole degrees of freedom (second order of H) when dividing $q_y(3q_x^2 - q_y^2)$ as $2q_x \times (q_x q_y) + q_y \times (q_x^2 - q_y^2)$. As the symmetry $q_x q_y$ and $q_x^2 - q_y^2$ are the same as $H_x H_y$ and $H_x^2 - H_y^2$, the $y(3x^2 - y^2)$ -type magnetic toroidal octupole gives rise to the coupling as $2q_x \times (H_x H_y) + q_y \times (H_x^2 - H_y^2) \sim q_x \sin(2\phi) + q_y \cos(2\phi)$. As q_x and q_y correspond to the polar vector, this decomposition expresses the emergence of in-plane magnetic toroidal dipoles $T_x \sim q_x$ and $T_y \sim q_y$ in the canted AFM state, and explains a qualitative behavior of the result in Figs. 2(c)-(f) and 3(a). Such an emergent magnetic toroidal dipole in the canted AFM state is consistent with the symmetry analysis by using the cluster multipole theory [54]. From the viewpoint of model parameters, the symmetric anisotropic exchange interaction is essential, since it breaks continuous spin rotational symmetry. The threefold symmetric interaction consists of the product of the dipole and quadrupole degrees of freedom on the basis of the microscopic multipole description [53, 55]. Recently, a similar angle-dependent magneto-electric effect observed in $\text{Co}_4\text{Nb}_2\text{O}_9$ [56, 57] is understood from the multipole aspect [58, 59].

IV. SUMMARY

To summarize, we have investigated the behavior of nonreciprocal magnon induced by the nearest-neighbor symmetric anisotropic exchange interaction on a honeycomb AFM. The antisymmetric nature of magnon bands is qualitatively different from that by the DM interaction. Moreover, we have found that the nonreciprocal magnon excitations exhibit peculiar angle-dependent responses under the external magnetic field. We have also clarified that the nonreciprocal dispersions and angle-dependent responses are related with the emergence of odd-parity magnetic toroidal multipoles, which are accompanied by the cluster AFM structure. As the antisymmetric modulation of the magnon bands becomes larger while increasing the bond-dependent symmetric anisotropic exchange interaction, the superexchange paths favoring the anisotropic interactions rather than the Heisenberg interaction, such as the Kitaev interaction [60], will enhance nonreciprocal physical phenomena.

Our mechanism of nonreciprocal magnons is expected to be observed in various honeycomb AFMs including the transition-metal tricalcogenide MnPS_3 [61–64] and rare-earth metallic compound ErNi_3Ga_9 [65], where the z -AFM state becomes the ground state. In these materials, the nonreciprocal magnon excitations will be observed in both microscopic and macroscopic experiments. Microscopically, the nonreciprocal magnon spectra can be detected by the inelastic neutron scattering experiment. On the other hand, from a macroscopic viewpoint, the angle-dependent nonreciprocal magneto-optical and nonreciprocal spin Seebeck effects can be observed under an in-plane magnetic field. As the nature of the asymmetric deformation of the magnon band is qualitatively different from that by the DM interaction, our mechanism will provide a deep understanding of further nonreciprocal magnon physics.

ACKNOWLEDGMENTS

We would like to thank T. J. Sato for fruitful discussions. This research was supported by JSPS KAKENHI Grants Numbers JP18H04296 (J-Physics), JP18K13488, JP19K03752, and JP19H01834. This work was also supported by the Toyota Riken Scholarship. Parts of the numerical calculations were performed in the supercomputing systems in ISSP, the University of Tokyo.

Appendix A: Ground-state spin configuration

In this Appendix, we show that the collinear AFM orderings with the z spin component are stabilized for $H = 0$ and the canted AFM ordering are stabilized for $\mathbf{H} = H(\cos\phi, \sin\phi, 0)$ by assuming the two-sublattice ordering and $J^z > J > 0$. We use four variational parameters $(\theta_A, \phi_A, \theta_B, \phi_B)$ representing the η (= A and B)-sublattice

spin state: $\mathbf{S}_\eta = S(\sin\theta_\eta \cos\phi_\eta, \sin\theta_\eta \sin\phi_\eta, \cos\theta_\eta)$. Then, the spin Hamiltonian in Eq. (1) is rewritten as

$$\mathcal{H} = \frac{3NS^2}{2} [J \sin\theta_A \sin\theta_B \cos(\phi_A - \phi_B) + J^z \cos\theta_A \cos\theta_B], \quad (\text{A1})$$

where N is the number of total spins. For $J^z > J > 0$, the staggered collinear AFM order is stabilized to satisfy $\theta_A = \theta$, $\theta_B = \pi - \theta$, $\phi_A = \phi$, and $\phi_B = \pi + \phi$. Then, Eq. (A1) reduces to

$$\mathcal{H} = -\frac{3NS^2}{2} [(J^z - J) \cos^2\theta + J]. \quad (\text{A2})$$

Thus, the ground state is realized at $\theta = 0$ or π when $J^z > J$.

Next, we show the optimal spin configuration under \mathbf{H} . To gain the Zeeman energy, the staggered AFM moment along the z direction is canted along the magnetic-field direction, whose spin ansatz is represented by $\mathbf{S}_{iA} = S(\sin\theta \cos\phi, \sin\theta \sin\phi, \cos\theta)$ and $\mathbf{S}_{iB} = S(\sin\theta \cos\phi, \sin\theta \sin\phi, -\cos\theta)$. Then, the spin Hamiltonian in Eq. (1) is rewritten as

$$\mathcal{H} = \frac{N}{2} \left\{ 3S^2(J^z + J) \left[\sin\theta - \frac{H}{3S(J^z + J)} \right]^2 - 3S^2J^z - \frac{H^2}{3(J^z + J)} \right\}. \quad (\text{A3})$$

By minimizing the ground state energy of the model in Eq. (A3) with respect to θ , the optimal canted value of θ is obtained by $\theta = \sin^{-1}[H/3S(J + J^z)]$. The spin waves in Sec. III are calculated for the obtained spin configurations.

Appendix B: Nonreciprocal magnons in the presence of the Dzyaloshinskii-Moriya interaction

In this Appendix, we discuss nonreciprocal magnons induced by the DM interaction for comparison. The localized spin model including the next-nearest-neighbor interaction in the honeycomb structure is given by

$$\begin{aligned} \mathcal{H} = & \sum_{\langle ij \rangle} \left[J(S_{iA}^+ S_{jB}^- + S_{iA}^- S_{jB}^+) + J^z S_{iA}^z S_{jB}^z \right] \\ & + \sum_{i,j} D (\mathbf{S}_{iA} \times \mathbf{S}_{jA} - \mathbf{S}_{iB} \times \mathbf{S}_{jB})^z - \sum_{i,\eta} \mathbf{H} \cdot \mathbf{S}_{i\eta}. \end{aligned} \quad (\text{B1})$$

We here take into account the DM interaction appearing in the next-nearest-neighbor spins instead of J^a in the model in Eq. (1), as shown in Fig 4(a). The collinear AFM ordering along the z direction is stabilized in the model in Eq. (B1) by choosing the parameter $J^z > J \gg D$.

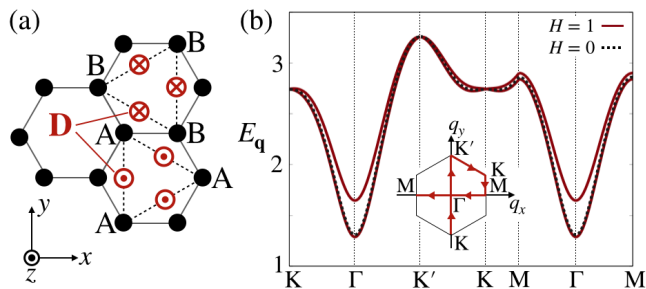


FIG. 4. (a) The DM vector in the honeycomb structure. (b) The magnon dispersions in the model in Eq. (B1) at $(J, J^z, D) = (0.9, 1, 0.05)$. The red solid (black dotted) lines represent the result at $H = 1$ ($H = 0$). In the inset, the first Brillouin zone is shown.

Figure 4(b) shows the magnon dispersion for nonzero $D = 0.05$ at $H = 1$ (red solid line) and $H = 0$ (black dotted line). The black dotted line shows magnon-band inclination on K- Γ -K' line by DM interaction. The red solid line shows the result in the presence of the in-plane magnetic field independent of the field direction. This tendency is clearly different from that by the symmetric anisotropic exchange interaction, which gives rise to direction-dependent nonreciprocal dispersions, in Sec. III B as well as that in the other nonreciprocal systems mentioned in the introduction [11, 20, 21, 26, 27, 38–42].

-
- [1] Curie, P., Sur la symétrie dans les phénomènes physiques, symétrie d'un champ électrique et d'un champ magnétique, *J. Phys. Theor. Appl.* **3**, 393 (1894).
- [2] M. Fiebig, Revival of the magnetoelectric effect, *J. Phys. D: Appl. Phys.* **38**, R123 (2005).
- [3] D. Khomskii, Trend: Classifying multiferroics: Mechanisms and effects, *Physics* **2**, 20 (2009).
- [4] R. Wakatsuki, Y. Saito, S. Hoshino, Y. M. Itahashi, T. Ideue, M. Ezawa, Y. Iwasa, and N. Nagaosa, Nonreciprocal charge transport in noncentrosymmetric superconductors, *Sci. Adv.* **3**, e1602390 (2017).
- [5] M. Mochizuki and S. Seki, Magnetolectric resonances and predicted microwave diode effect of the skyrmion crystal in a multiferroic chiral-lattice magnet, *Phys. Rev. B* **87**, 134403 (2013).
- [6] H. Saito, K. Uenishi, N. Miura, C. Tabata, H. Hidaka, T. Yanagisawa, and H. Amitsuka, Evidence of a new current-induced magnetoelectric effect in a toroidal magnetic ordered state of UNi_4B , *J. Phys. Soc. Jpn.* **87**, 033702 (2018).
- [7] Y. Shiomi, T. Akiba, H. Takahashi, and S. Ishiwata, Giant piezoelectric response in superionic polar semiconductor, *Adv. Electron. Mater.* **4** (2018).
- [8] Y. Shiomi, H. Watanabe, H. Masuda, H. Takahashi, Y. Yanase, and S. Ishiwata, Observation of a magnetopiezoelectric effect in the antiferromagnetic metal EuMnBi_2 , *Phys. Rev. Lett.* **122**, 127207 (2019).
- [9] R. L. Melcher, Linear contribution to spatial dispersion in the spin-wave spectrum of ferromagnets, *Phys. Rev. Lett.* **30**, 125 (1973).
- [10] M. Kataoka, Spin waves in systems with long period helical spin density waves due to the antisymmetric and symmetric exchange interactions, *J. Phys. Soc. Jpn.* **56**, 3635 (1987).
- [11] D. Cortés-Ortuño and P. Landeros, Influence of the Dzyaloshinskii-Moriya interaction on the spin-wave spectra of thin films, *J. Phys.: Condens. Matter* **25**, 156001 (2013).
- [12] J.-H. Moon, S.-M. Seo, K.-J. Lee, K.-W. Kim, J. Ryu, H.-W. Lee, R. D. McMichael, and M. D. Stiles, Spin-wave propagation in the presence of interfacial Dzyaloshinskii-Moriya interaction, *Phys. Rev. B* **88**, 184404 (2013).
- [13] S. Hayami, H. Kusunose, and Y. Motome, Asymmetric magnon excitation by spontaneous toroidal ordering, *J. Phys. Soc. Jpn.* **85**, 053705 (2016).
- [14] D. Ghader and A. Khater, A new class of nonreciprocal spin waves on the edges of 2d antiferromagnetic honeycomb nanoribbons, *Sci. Rep.* **9**, 2045 (2019).
- [15] M. Kawano, Y. Onose, and C. Hotta, Designing Rashba-Dresselhaus effect in magnetic insulators, *Commun. Phys.* **2**, 27 (2019).
- [16] M. Kawano and C. Hotta, Discovering momentum-dependent magnon spin texture in insulating antiferromagnets: Role of the Kitaev interaction, *Phys. Rev. B* **100**, 174402 (2019).
- [17] I. Dzyaloshinsky, A thermodynamic theory of weak ferromagnetism of antiferromagnetics, *J. Phys. Chem. Solids* **4**, 241 (1958).
- [18] T. Moriya, Anisotropic superexchange interaction and weak ferromagnetism, *Phys. Rev.* **120**, 91 (1960).
- [19] Y. Iguchi, S. Uemura, K. Ueno, and Y. Onose, Nonreciprocal magnon propagation in a noncentrosymmetric ferromagnet LiFe_5O_8 , *Phys. Rev. B* **92**, 184419 (2015).
- [20] V. L. Zhang, K. Di, H. S. Lim, S. C. Ng, M. H. Kuok, J. Yu, J. Yoon, X. Qiu, and H. Yang, In-plane angular dependence of the spin-wave nonreciprocity of an ultrathin film with Dzyaloshinskii-Moriya interaction, *Appl. Phys. Lett.* **107**, 022402 (2015).
- [21] J. Cho, N.-H. Kim, S. Lee, J.-S. Kim, R. Lavrijsen, A. Solignac, Y. Yin, D.-S. Han, N. J. Van Hoof, H. J. Swagten, *et al.*, Thickness dependence of the interfacial Dzyaloshinskii-Moriya interaction in inversion symmetry broken systems, *Nat. Commun.* **6**, 1 (2015).
- [22] T. J. Sato, D. Okuyama, T. Hong, A. Kikkawa, Y. Taguchi, T.-h. Arima, and Y. Tokura, Magnon dispersion shift in the induced ferromagnetic phase of noncentrosymmetric MnSi , *Phys. Rev. B* **94**, 144420 (2016).
- [23] S. Seki, Y. Okamura, K. Kondou, K. Shibata, M. Kubota, R. Takagi, F. Kagawa, M. Kawasaki, G. Tatara, Y. Otani, and Y. Tokura, Magnetochiral nonreciprocity of volume spin wave propagation in chiral-lattice ferromagnets, *Phys. Rev. B* **93**, 235131 (2016).
- [24] G. Gitgeatpong, Y. Zhao, P. Piyawongwatthana, Y. Qiu, L. W. Harriger, N. P. Butch, T. J. Sato, and K. Matan, Nonreciprocal magnons and symmetry-breaking in the noncentrosymmetric antiferromagnet,

- Phys. Rev. Lett. **119**, 047201 (2017).
- [25] R. Takagi, D. Morikawa, K. Karube, N. Kanazawa, K. Shibata, G. Tatara, Y. Tokunaga, T. Arima, Y. Taguchi, Y. Tokura, and S. Seki, Spin-wave spectroscopy of the Dzyaloshinskii-Moriya interaction in room-temperature chiral magnets hosting skyrmions, Phys. Rev. B **95**, 220406(R) (2017).
- [26] S. Tacchi, R. E. Troncoso, M. Ahlberg, G. Gubbiotti, M. Madami, J. Åkerman, and P. Landeros, Interfacial Dzyaloshinskii-Moriya interaction in Pt/CoFeB films: effect of the heavy-metal thickness, Phys. Rev. Lett. **118**, 147201 (2017).
- [27] A. K. Chaurasiya, S. Choudhury, J. Sinha, and A. Barman, Dependence of interfacial Dzyaloshinskii-Moriya interaction on layer thicknesses in Ta/Co-Fe-B/TaO_x heterostructures from Brillouin light scattering, Phys. Rev. Appl. **9**, 014008 (2018).
- [28] Y. Iguchi, Y. Nii, M. Kawano, H. Murakawa, N. Hanasaki, and Y. Onose, Microwave nonreciprocity of magnon excitations in the noncentrosymmetric antiferromagnet Ba₂MnGe₂O₇, Phys. Rev. B **98**, 064416 (2018).
- [29] Y. Takahashi, R. Shimano, Y. Kaneko, H. Murakawa, and Y. Tokura, Magnetoelectric resonance with electromagnons in a perovskite helimagnet, Nat. Phys. **8**, 121 (2011).
- [30] S. Miyahara and N. Furukawa, Nonreciprocal directional dichroism and toroidalmagnons in helical magnets, J. Phys. Soc. Jpn. **81**, 023712 (2012).
- [31] S. Miyahara and N. Furukawa, Electromagnon in multiferroic materials with Dzyaloshinsky-Moriya-interaction-induced helical spin structures, J. Korean Phys. Soc. **62**, 1763 (2013).
- [32] S. Miyahara and N. Furukawa, Theory of magneto-optical effects in helical multiferroic materials via toroidal magnon excitation, Phys. Rev. B **89**, 195145 (2014).
- [33] M. Mochizuki, Microwave magnetochiral effect in Cu₂OSeO₃, Phys. Rev. Lett. **114**, 197203 (2015).
- [34] I. Proskurin, A. S. Ovchinnikov, J.-i. Kishine, and R. L. Stamps, Excitation of magnon spin photocurrents in antiferromagnetic insulators, Phys. Rev. B **98**, 134422 (2018).
- [35] N. Okuma, Nonreciprocal superposition state in antiferromagnetic optospintronics, Phys. Rev. B **99**, 094401 (2019).
- [36] R. Takashima, Y. Shiomi, and Y. Motome, Nonreciprocal spin Seebeck effect in antiferromagnets, Phys. Rev. B **98**, 020401(R) (2018).
- [37] Y. Shiomi, R. Takashima, D. Okuyama, G. Giteatpong, P. Piyawongwatthana, K. Matan, T. J. Sato, and E. Saitoh, Spin Seebeck effect in the polar antiferromagnet α -Cu₂V₂O₇, Phys. Rev. B **96**, 180414(R) (2017).
- [38] P. Grünberg, R. Schreiber, Y. Pang, M. B. Brodsky, and H. Sowers, Layered magnetic structures: Evidence for antiferromagnetic coupling of Fe layers across Cr interlayers, Phys. Rev. Lett. **57**, 2442 (1986).
- [39] P. X. Zhang and W. Zinn, Spin-wave modes in antiparallel magnetized ferromagnetic double layers, Physical Review B **35**, 5219 (1987).
- [40] K. Di, S. Feng, S. N. Piramanayagam, V. Zhang, H. S. Lim, S. C. Ng, and M. H. Kuok, Enhancement of spin-wave nonreciprocity in magnonic crystals via synthetic antiferromagnetic coupling, Sci. Rep. **5**, 10153 (2015).
- [41] R. A. Gallardo, T. Schneider, A. K. Chaurasiya, A. Oelschlägel, S. S. P. K. Arekapudi, A. Roldán-Molina, R. Hübner, K. Lenz, A. Barman, J. Fassbender, J. Lindner, O. Hellwig, and P. Landeros, Reconfigurable spin-wave nonreciprocity induced by dipolar interaction in a coupled ferromagnetic bilayer, Phys. Rev. Appl. **12**, 034012 (2019).
- [42] E. Albisetti, S. Tacchi, R. Silvani, G. Scaramuzzi, S. Finizio, S. Wintz, C. Rinaldi, M. Cantoni, J. Raabe, G. Carlotti, *et al.*, Optically inspired nanomagnonics with nonreciprocal spin waves in synthetic antiferromagnets, Adv. Mater. , 1906439 (2020).
- [43] S. Cheon, H.-W. Lee, and S.-W. Cheong, Nonreciprocal spin waves in a chiral antiferromagnet without the Dzyaloshinskii-Moriya interaction, Phys. Rev. B **98**, 184405 (2018).
- [44] P. A. Maksimov, Z. Zhu, S. R. White, and A. L. Chernyshev, Anisotropic-exchange magnets on a triangular lattice: spin waves, accidental degeneracies, and dual spin liquids, Physical Review X **9**, 021017 (2019).
- [45] J. A. Otálora, M. Yan, H. Schultheiss, R. Hertel, and A. Kákay, Curvature-induced asymmetric spin-wave dispersion, Phys. Rev. Lett. **117**, 227203 (2016).
- [46] R. Gallardo, P. Alvarado-Seguel, T. Schneider, C. Gonzalez-Fuentes, A. Roldán-Molina, K. Lenz, J. Lindner, and P. Landeros, Spin-wave non-reciprocity in magnetization-graded ferromagnetic films, New J. Phys. **21**, 033026 (2019).
- [47] Y.-D. Li, X. Wang, and G. Chen, Anisotropic spin model of strong spin-orbit-coupled triangular antiferromagnets, Phys. Rev. B **94**, 035107 (2016).
- [48] X. S. Wang, Y. Su, and X. R. Wang, Topologically protected unidirectional edge spin waves and beam splitter, Phys. Rev. B **95**, 014435 (2017).
- [49] X. S. Wang, H. W. Zhang, and X. R. Wang, Topological magnonics: A paradigm for spin-wave manipulation and device design, Phys. Rev. Applied **9**, 024029 (2018).
- [50] J. Colpa, Diagonalization of the quadratic boson hamiltonian, Physica A **93**, 327 (1978).
- [51] N. A. Spaldin, M. Fiebig, and M. Mostovoy, The toroidal moment in condensed-matter physics and its relation to the magnetoelectric effect, J. Phys.: Condens. Matter **20**, 434203 (2008).
- [52] S. Hayami and H. Kusunose, Microscopic description of electric and magnetic toroidal multipoles in hybrid orbitals, Journal of the Physical Society of Japan **87**, 033709 (2018).
- [53] S. Hayami, M. Yatsushiro, Y. Yanagi, and H. Kusunose, Classification of atomic-scale multipoles under crystallographic point groups and application to linear response tensors, Phys. Rev. B **98**, 165110 (2018).
- [54] M.-T. Suzuki, T. Nomoto, R. Arita, Y. Yanagi, S. Hayami, and H. Kusunose, Multipole expansion for magnetic structures: A generation scheme for a symmetry-adapted orthonormal basis set in the crystallographic point group, Phys. Rev. B **99**, 174407 (2019).
- [55] M. Matsumoto, K. Chimata, and M. Koga, Symmetry analysis of spin-dependent electric dipole and its application to magnetoelectric effects, Journal of the Physical Society of Japan **86**, 034704 (2017).
- [56] N. D. Khanh, N. Abe, H. Sagayama, A. Nakao, T. Hanashima, R. Kiyonagi, Y. Tokunaga, and T. Arima, Magnetoelectric coupling in the honeycomb antiferromagnet Co₄Nb₂O₉, Phys. Rev. B **93**, 075117 (2016).
- [57] N. D. Khanh, N. Abe, S. Kimura, Y. Tokunaga, and T. Arima, Manipulation of electric polarization with ro-

- tating magnetic field in a honeycomb antiferromagnet $\text{Co}_4\text{Nb}_2\text{O}_9$, *Phys. Rev. B* **96**, 094434 (2017).
- [58] Y. Yanagi, S. Hayami, and H. Kusunose, Manipulating the magnetoelectric effect: Essence learned from $\text{Co}_4\text{Nb}_2\text{O}_9$, *Phys. Rev. B* **97**, 020404(R) (2018).
- [59] M. Matsumoto and M. Koga, Symmetry analysis of magnetoelectric effects in honeycomb antiferromagnet $\text{Co}_4\text{Nb}_2\text{O}_9$, *J. Phys. Soc. Jpn.* **88**, 094704 (2019).
- [60] G. Jackeli and G. Khaliullin, Mott insulators in the strong spin-orbit coupling limit: From Heisenberg to a quantum compass and Kitaev models, *Phys. Rev. Lett.* **102**, 017205 (2009).
- [61] E. Ressouche, M. Loire, V. Simonet, R. Ballou, A. Stunault, and A. Wildes, Magnetoelectric MnPS_3 as a candidate for ferrotoroidicity, *Phys. Rev. B* **82**, 100408(R) (2010).
- [62] X. Li, T. Cao, Q. Niu, J. Shi, and J. Feng, Coupling the valley degree of freedom to antiferromagnetic order, *Proc. Natl. Acad. Sci.* **110**, 3738 (2013).
- [63] N. Sivadas, M. W. Daniels, R. H. Swendsen, S. Okamoto, and D. Xiao, Magnetic ground state of semiconducting transition-metal trichalcogenide monolayers, *Phys. Rev. B* **91**, 235425 (2015).
- [64] Y. Shiomi, R. Takashima, and E. Saitoh, Experimental evidence consistent with a magnon Nernst effect in the antiferromagnetic insulator MnPS_3 , *Phys. Rev. B* **96**, 134425 (2017).
- [65] H. Ninomiya, T. Sato, Y. Matsumoto, T. Moyoshi, A. Nakao, K. Ohishi, Y. Kousaka, J. Akimitsu, K. Inoue, and S. Ohara, Neutron diffraction study of antiferromagnetic ErNi_3Ga_9 in magnetic fields, *Physica B* **536**, 392 (2018).